Int. J. Heat Mass Transfer. Vol. 30, No. 6, pp. 1209–1222, 1987
Printed in Great Britain

0017-9310/87 $3.00 + 0.00

A study of laminar natural convection in a non-uniformly heated annular fluid layer

M. PRUD'HOMME, L. ROBILLARD and P. VASSEUR

Génie mécanique, Ecole Polytechnique de Montréal, C.P. 6079, Succ. "A", Montréal, Québec, Canada H3C 3A7

(*Received* 7 *May* 1986 *and in final form* 29 *October* 1986)

Abstract—A study is made of free convection in an annular fluid layer confined between two horizontal cylinders. Results are presented for the case of an adiabatic inner boundary with a sinusoidal temperature distribution on the outer boundary. The problem is formulated in terms of the Boussinesq approximations and solved using perturbation and finite-difference techniques. It is found that the results obtained from both methods are in good mutual agreement for weak convection. The solutions reveal the existence of various flow regimes, depending on Ra and the angular position of the temperature maximum on the outer boundary, which are similar in character to earlier results for the porous medium. It is found that incipient convection may decrease Nu in one case. In particular, when heating is from below, three distinct subregimes may be obtained within the range of parameters considered ($R = 2$, $0 < Ra < 40{,}000$) namely, the steady quadri-cellular flow for $Ra < 1120$, the circulating flow with or without secondary cells for $1120 < Ra < 40{,}000$, and finally unsteady circulating flow for $Ra > 40{,}000$. Secondary cells begin to appear near the outer boundary at $Ra = 11{,}000$. For an arbitrary heating angle, there is always a net circulating flow around the cavity, unless heating is from the top, which leads to an enhancement of heat transfer with the surroundings. The maximum flow and heat transfer rates are obtained for a heating angle below the horizontal whose value depends on Ra.

1. INTRODUCTION

NATURAL convection flow within closed loop cavities is involved in numerous industrial processes as a means of transporting thermal energy. The applications range from the cooling of turbine blades to the maintenance of icefree navigation buoys and are reviewed in detail by Japikse [1]. The subject, as can be expected, constitutes an important current research topic. In particular, much attention has been devoted lately to the toroidal thermosyphon following the pioneering work of Welander [2]. This particular problem has been studied both theoretically and experimentally under various thermal boundary conditions.

Creveling *et al.* [3] and subsequently Damerell and Schoenhals [4] reported unsteadiness and flow reversals in the case of a vertical toroidal loop. In order to predict these phenomena, theoretical studies were performed based on a one-dimensional approach to the system of momentum and energy equations. This one-dimensional approach applied to an essentially three-dimensional situation turned out to be incapable of predicting important features of the flow. Mertol *et al.* [5, 6] proposed instead a less restrictive, two-dimensional axially symmetric model. Still, their two-dimensional model could not predict the experimentally observed recirculation zones near the surface of the tube.

Singh and Elliot [7] considered the problem of natural convection between two horizontal concentric cylinders, which, unlike the toroidal problem, may be described exactly by two-dimensional equations. This simpler problem is known to exhibit the same kind of flow behavior (unsteadiness, recirculation zones) as the toroidal configuration and thus offers an alternative way of understanding the features of the latter. However, the perturbation solution of ref. [7] is limited to the case of stable vertical stratification with symmetry with respect to the vertical diameter for which no net circulating flow exists around the cavity.

The case of two horizontal concentric cylinders filled with a porous medium and subjected to an arbitrarily oriented thermal stratification at the outer boundary was investigated by Robillard *et al.* [8, 9]. Their studies showed that the symmetry hypothesis with respect to the vertical diameter cannot be applied in general and that one must allow for the possibility of a net circulating flow around the annular cavity. They found out that different flow regimes were possible depending on the Rayleigh number and the orientation of the thermal stratification with respect to gravity. Namely, there could be steady multicellular flow, unsteady periodic multicellular flow and finally unsteady chaotic flow. These authors have also studied separately the situation where heating is from below [10], in which case the circulating flow in the loop could develop in either direction with equal probability.

The present study is focused upon the problem of natural convection in a fluid layer confined between two horizontal concentric cylinders. It represents the natural extension of the work of ref. [9] from a porous medium to a fluid medium. The problem is formulated

NOMENCLATURE

C	specific heat [J kg^{-1} K^{-1}]
G	Grashof number, $\beta\Delta T' r_o'^3 g/\nu^2$
g	gravitational acceleration [m s^{-2}]
k	thermal conductivity [J s^{-1} m^{-1} K^{-1}]
Nu	overall Nusselt number defined by equations (28) and (29)
Nu^*	Nusselt number for pure conduction
P	fluid pressure [N m^{-2}]
Pr	Prandtl number, ν/α
r'	radial coordinate [m]
R	aspect ratio, r_o'/r_i'
Ra	Rayleigh number, $G\,Pr$
t'	time [s]
T'	temperature [K]
$\Delta T'$	half the temperature difference between the hottest and coldest points on the outer boundary
u'	velocity component in the r'-direction [m s^{-1}]
V'	velocity [m s^{-1}]
v'	velocity component in the ϕ'-direction [m s^{-1}].

Greek symbols

α	diffusivity [m^2 s^{-1}]
β	thermal expansion coefficient [K^{-1}]
μ	dynamic viscosity [kg m^{-1} s^{-1}]
ν	kinematic viscosity [m^2 s^{-1}]
ρ'	density [kg m^{-3}]
ϕ	angular coordinate
ϕ_o	heating angle
ψ	dimensionless stream function, ψ'/ν
ω'	vorticity [s^{-1}].

Superscripts

$'$	dimensional variable
n	latest available field value.

Subscripts

i	value on inner cylinder
o	value on outer cylinder.

Other symbols

$\nabla' \cdot ( )$ divergence operator
$\nabla'( )$ gradient operator
$\nabla'^2( )$ Laplacian operator.

in terms of the usual Boussinesq approximations and treated by analytical and numerical methods. The set of governing equations is solved for a zero heat flux boundary condition on the inner wall and a sinusoidal temperature distribution on the outer wall. Previous experience with the porous medium [10] has shown that adiabatic conditions at the inner wall allow the existence of a steady flow regime with a net circulation when the cavity is heated from below, unlike isothermal conditions which always lead to oscillating flow patterns.

Results are presented which reveal the existence of various distinct flow regimes and the enhancement of heat transfer rates by the net circulation which is established around the annular cavity. The concluding remarks emphasize the particular aspects which distinguish the fluid medium case from the porous.

2. MATHEMATICAL MODEL

Figure 1 shows the geometry of the problem. The annular region between the two concentric cylinders represents the flow domain of interest for the present analysis. A zero heat flux (i.e. adiabatic) condition is imposed on the inner boundary, while a temperature distribution of the form

$$T_o' - T_i' = \Delta T' \cos(\phi - \phi_o) \tag{1}$$

is prescribed on the outer boundary.

The governing non-dimensional equations for a single-phase fluid with constant properties which satisfies the Boussinesq approximations are, after scaling time, length, temperature, velocity and pressure with $\rho_i' r_o'^2/\mu$, r_o', $\Delta T'$, $\mu/\rho_i' r_o'$ and $\mu^2/\rho_i' r_o'^3$

$$\nabla \cdot \mathbf{V} = 0 \tag{2}$$

$$\frac{\partial \mathbf{V}}{\partial t} + (\mathbf{V}\cdot\nabla)\mathbf{V} = -\frac{G}{R^3 g} T\mathbf{g} - \nabla p + \nabla^2 \mathbf{V} \tag{3}$$

$$\frac{\partial T}{\partial t} + (\mathbf{V}\cdot\nabla)T = \frac{1}{Pr}\nabla^2 T. \tag{4}$$

The corresponding set of dimensionless boundary conditions is simply

$$\frac{\partial T}{\partial r} = 0, \quad \mathbf{V} = 0 \quad \text{for} \quad r = 1 \tag{5a}$$

$$T = \cos(\phi - \phi_o), \quad \mathbf{V} = 0 \quad \text{for} \quad r = R. \tag{5b}$$

The pressure term can be eliminated in the usual way by taking the curl of equation (3) which then becomes

$$\frac{\partial \omega}{\partial t} + (\mathbf{V}\cdot\nabla)\omega = -\frac{G}{R^3}\mathscr{L}(T) + \nabla^2\omega \tag{6}$$

where

$$\mathscr{L} = \sin\phi \frac{\partial}{\partial r} + \frac{\cos\phi}{r}\frac{\partial}{\partial \phi}.$$

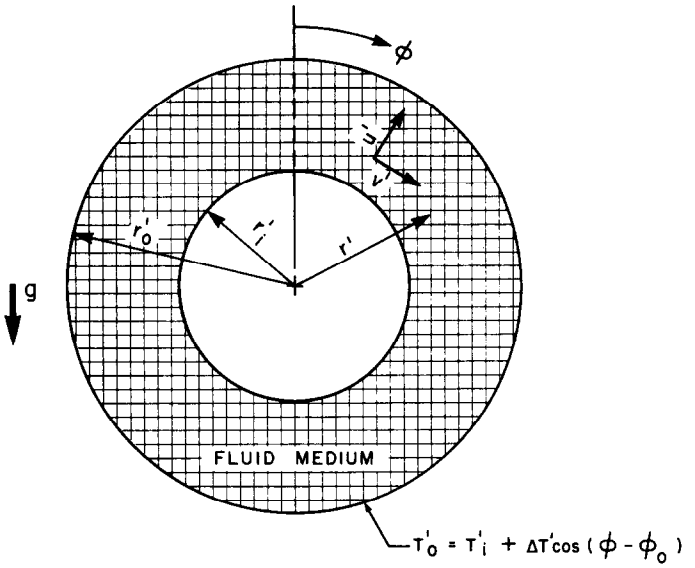

FIG. 1. Flow geometry and coordinate system.

The velocity components and the vorticity may be expressed in terms of the dimensionless stream function ψ as

$$u = \frac{1}{r}\frac{\partial \psi}{\partial \phi} \tag{7a}$$

$$v = -\frac{\partial \psi}{\partial r} \tag{7b}$$

$$\omega = -\nabla^2 \psi. \tag{7c}$$

In this case equation (2) is identically satisfied, while equations (4) and (6) become respectively

$$\nabla^2 T = \frac{Pr}{r}\left[\frac{\partial \psi}{\partial \phi}\frac{\partial T}{\partial r} - \frac{\partial \psi}{\partial r}\frac{\partial T}{\partial \phi}\right] + Pr\frac{\partial T}{\partial t} \tag{8}$$

and

$$\nabla^4 \psi = \frac{1}{r}\left[-\frac{\partial \psi}{\partial r}\frac{\partial \nabla^2 \psi}{\partial \phi} + \frac{\partial \psi}{\partial \phi}\frac{\partial \nabla^2 \psi}{\partial r}\right] - \frac{G}{R^3}\mathscr{L}(T) + \frac{\partial \nabla^2 \psi}{\partial t}. \tag{9}$$

It is appropriate to point out that there may be a net circulating flow around the annulus. Consequently the value of ψ may be arbitrarily fixed on only one of the two boundaries. Assuming that

$$\psi = \psi_i \quad \text{for} \quad r = 1 \tag{10a}$$

$$\psi = 0 \quad \text{for} \quad r = R \tag{10b}$$

ψ_i corresponds then to the net flow rate around the annular region whose value has yet to be determined.

Two other boundary conditions for ψ follow at once from equations (5). The tangential velocity must vanish at the walls which requires that ψ must satisfy

$$\frac{\partial \psi}{\partial r} = 0 \quad \text{for} \quad r = 1 \tag{11a}$$

$$\frac{\partial \psi}{\partial r} = 0 \quad \text{for} \quad r = R. \tag{11b}$$

A fourth boundary condition for ψ may be obtained by taking advantage of the known temperature distribution at $r = R$. Integrating equation (3) around the outer boundary yields the following integral relation

$$\int_0^{2\pi} \nabla^2 \frac{\partial \psi}{\partial r}\bigg|_{r=R} d\phi = -\frac{G\pi}{R^3}\sin \phi_o. \tag{12}$$

As long as the flow is steady, one can get another integral relation for ψ at $r = 1$ from the zero heat flux condition at the inner wall. Taking the gradient of equation (3) in the radial direction and integrating the result around the inner boundary using the periodicity of the problem leads to

$$\int_0^{2\pi} \frac{\partial^2 \nabla^2 \psi}{\partial r^2}\bigg|_{r=1} d\phi = 0. \tag{13}$$

3. METHODS OF SOLUTION

Solutions to the governing equations will now be sought by analytical and numerical methods. Regular perturbation techniques will be used for weak flows, that is, when the Rayleigh number is small. Steady-state low order solutions, valid in the limit as *Ra* tends towards zero, will be obtained. The pure conduction temperature distribution will be taken as the initial unperturbed state. The analytical approach serves two purposes. First, it will be used to put forward some

general tendencies of the flow in the annular layer under the influence of natural convection. Second, it will provide an initial test for the numerical approach which is required at Rayleigh values where the perturbation analysis is no longer valid. Numerical solutions will be obtained using finite-difference techniques and allowing for unsteadiness in order to determine the critical value of Ra above which the flow becomes time dependent.

3.1. *Perturbation solution*

The system of equations (8) and (9) together with boundary conditions (5) for T and equations (10b), (11) and (12) or (13) for ψ defines a regular perturbation problem. As only steady solutions are sought, the unsteady terms in equations (8) and (9) will not be considered any further.

One seeks a power series solution of the form

$$\psi(r,\phi) = \sum_{n=0}^{\infty} (G/R^3)^n \psi_n(r,\phi) \tag{14a}$$

$$T(r,\phi) = \sum_{n=0}^{\infty} (G/R^3)^n T_n(r,\phi). \tag{14b}$$

Substituting equations (14) into equations (8) and (9) and collecting like powers of G yields a sequence of linear equations

$$\nabla^4\psi_n + \sum_{i=0}^{n} \frac{1}{r}\left(\frac{\partial\psi_i}{\partial r}\frac{\partial\nabla^2\psi_{n-i}}{\partial\phi} - \frac{\partial\psi_i}{\partial\phi}\frac{\partial\nabla^2\psi_{n-i}}{\partial r}\right) = -\mathscr{L}(T_{n-1}), \quad n = 1,2,\ldots \tag{15a}$$

$$\nabla^2 T_n = \frac{Pr}{r}\sum_{i=0}^{n}\frac{\partial\psi_i}{\partial\phi}\frac{\partial T_{n-i}}{\partial r} - \frac{\partial\psi_i}{\partial r}\frac{\partial T_{n-i}}{\partial\phi}, \quad n = 0,1,\ldots \tag{15b}$$

The zero-order solution corresponds to the pure conduction situation in which case $\psi_0 = 0$ and

$$T_0 = A(r + r^{-1})\cos(\phi - \phi_o) \tag{16}$$

where $A = R/(R^2+1)$. The first-order solution reads

$$\psi_1 = A\left\{c_1 + c_2\ln r + c_3 r^2\ln r + c_4 r^2 - \frac{r^4}{64}\right\}\sin\phi_o + A\left\{c_5 r^4 + c_6 r^2 + c_7 + c_8 r^{-2} - \frac{r^2}{16}\ln r\right\}\sin(2\phi - \phi_o) \tag{17a}$$

$$T_1 = \frac{Pr\,A^2}{4}[2f_1(r)\cos(3\phi - 2\phi_o) + f_2(r)\cos(\phi - 2\phi_o) + f_3(r)\cos\phi]. \tag{17b}$$

The functions f_i in equation (17b) are given explicitly in the Appendix along with the values of the constants c_i in equation (17a). The second-order solution is obtained from the lower order solutions in a straightforward manner. However, the calculations involved become rapidly prohibitive. For this reason, the second-order solution has been carried out only for the stream function. The result for the second-order stream function ψ_2 may be written in this form

$$\psi_2 = \frac{A^2}{2}[g_1(r)\sin(4\phi - 2\phi_o) + g_2(r)\sin(2\phi - 2\phi_o) + g_3(r)\sin(2\phi) + g_4(r)\sin(2\phi_o)]. \tag{18}$$

Further details are provided in the Appendix.

3.2. *Numerical solution*

Solutions for the flow field and the temperature distribution within the doubly-connected region may be found by standard numerical methods. The governing equations for the temperature, equation (4), vorticity, equation (6), and stream function, equation (7c), are first discretized according to the well-known central difference scheme for a regular mesh size. The discretized equations for T, ω and ψ are then solved twice at each time step, using the latest available field values, until convergence to a steady solution is achieved. Boundary conditions (5a) and (10) are used for T and ψ, respectively. For the vorticity equation, one uses the latest values of ω from equation (7c) on the boundaries to obtain the new field values.

The discretized Poisson equation for ψ is solved explicitly with a successive overrelaxation method (SOR) whereas the T and ω equations are solved using an alternating direction implicit method (ADI). Essentially, the ADI method solves for the new field values of a given variable by assuming explicit discretization of its governing equation in a single direction, say r, and explicit discretization otherwise.

The resultant set of finite-difference equations is tridiagonal in form and therefore both easy and economical to solve on the computer. The procedure is then repeated in the ϕ-direction, then in the r, and so on... Thus, the ADI method requires a boundary condition at the end points in both the r- and ϕ-directions. In the present case, the only physical condition to be used in the ϕ-direction is the periodicity. Referring to ref. [10] for details, solution in the ϕ-direction is obtained from 0 to 4π with the previous time step values at 2π used as boundary conditions at the end points. The procedure is repeated once more before saving the values between π and 3π. The results are independent of the origin for ϕ.

When the ψ equation is being solved, the value of ψ_1 is not known explicitly, but only implicitly through equation (12) or (13). In order to satisfy the latter, ψ_1'' must be adjusted iteratively as follows. Integrating $\mathbf{r}\wedge\partial\mathbf{V}/\partial t$ over the annulus using equation (3) and periodicity leads, after a few simplifications, to

$$\int_1^R\int_0^{2\pi} r^2\left[\frac{\partial^2\psi}{\partial t\,\partial r} + \frac{G}{R^3}T\sin\phi\right]dr\,d\phi = \int_0^{2\pi}\left[r^2\frac{\partial^2\psi}{\partial r^2}\right]_{r=1}^{r=R}d\phi \tag{19}$$

which expresses the torque equilibrium with respect

to the geometric center between the inertial, gravitational and viscous forces. Now, let $\Delta\psi$ be a correction stream function such that $\psi = \psi^n + \Delta\psi$ satisfies equation (19). A simple choice for such a function would be for instance

$$\Delta\psi = A_1 + A_2 r^2 + A_3 \ln r + A_4 r^2 \ln r \qquad (20)$$

where the A_i are determined at once in terms of $\Delta\psi_i$ with the help of equations (10) and (11). Substitution of equation (20) into equation (19) gives

$$\frac{8\pi(1-R^2)^2\Delta\psi_i}{4R^2\ln^2 R-(1-R^2)^2} = \int_1^R \int_0^{2\pi} r\left[\frac{\partial^2\psi^n}{\partial t\,\partial r} + \frac{GT}{R^3}\sin\phi\right] \times \mathrm{d}r\,\mathrm{d}\phi - \int_0^{2\pi}\left[\frac{r^2\,\partial^2\psi^n}{\partial r^2}\right]_{r=1}^{r=R}\mathrm{d}\phi. \qquad (21)$$

For fast convergence to a steady-state solution, one can use equation (21), with an appropriate relaxation factor, just once every time step. A similar procedure based directly on equation (12) instead of equation (19), although perfectly valid in principle, turned out to be unsatisfactory in practice. Let us point out that the correction with equation (21) needs to be applied only to ψ_i^n and not to the whole ψ^n field. Let us mention also briefly that the adiabatic boundary condition for the temperature equation is implemented at the inner wall using image points. The calculations were performed for an 18 by 36 finite-difference grid on an IBM 4831 computer. The average computing time required per run was around 5 min of CPU. The results were stored on disk after each run to be used as initial conditions for the next calculations. The accuracy of the numerical technique used in the present study has been discussed in detail in ref. [11].

4. RESULTS AND DISCUSSION

4.1. *Pseudo-conduction regime*

At low Rayleigh numbers, convective heat transfer is negligible within the annular fluid layer and the temperature distribution throughout the annulus is then determined essentially by conduction. This situation is called the pseudo-conduction regime.

It may now be shown from the perturbation solution that flow reversals near the boundaries are possible even in the limit of very small Rayleigh numbers, provided that ϕ_o (or $\pi-\phi_o$) is small enough. It is well known from boundary layer theory that the shear stress vanishes at the points where the flow will separate from or reattach to the walls. The angular locations of these points are thus related to the condition

$$\left.\frac{\partial v}{\partial r}\right|_{r=1 \text{ or } R} = 0. \qquad (22)$$

The latter may be expressed to first order in Ra from equation (17a). It is then easy to see that for a given value of R, say $R = 2$, flow reversals will occur on the outer boundary if $|\phi_o|$ or $|180°-\phi_o| \leqslant 3.2°$. Similarly, flow reversals will occur on the inner boundary if $|\phi_o|$ or $|180°-\phi_o| \leqslant 4.8°$. By comparison with the porous counterpart of the present problem [9], there is a wide range of ϕ_o over which no separation occurs at low Ra.

Thus for $R = 2$, there will be two pairs of vortices imbedded in a circulation flow around the annulus if $|\phi_o|$ or $|180°-\phi_o| \leqslant 3.2°$. For $|\phi_o|$ or $|\phi_o-180°|$ between 3.2° and 4.8° there remains only one pair of recirculation cells adjacent to the inner boundary. Finally, no separation can occur if $|\phi_o|$ or $|\phi_o-180°|$ is greater than 4.8° and the streamlines are then concentric circles. In this respect, the present problem admits solutions which are very similar in character to those which were given earlier by Robillard *et al.* [9] for an annular porous layer. The effect of retaining the second-order terms in equation (22) is to increase slightly the values of the critical angles given above. This tendency is moreover confirmed by the numerical solutions which reveal that the critical heating angle values will keep on increasing with Rayleigh number.

It should be mentioned that for the cases of heating from the top or the bottom of the cylinder, i.e. when $|\phi_o| = 0$ or π, there is no net circulation around the annular and then $\psi = 0$ on both boundaries. The streamlines form a four mirror-image cell pattern. This pattern corresponds to four counterrotating vortices which are symmetric with respect to both horizontal and vertical axes. These symmetry characteristics arise from the fact that governing equations (8) and (9), together with boundary conditions (5) and (10) become invariant under the transformations

$$(r, \phi, T, \psi \to r, -\phi, T, -\psi) \qquad (23a)$$

$$(r, \phi, T, \psi \to r, \pi-\phi, -T, -\psi). \qquad (23b)$$

The zero- and first-order perturbation solutions for temperature T_0, equation (16), and T_1, equation (17b), allow us to examine the effect of incipient convection on the heat transfer process. As a consequence of the adiabatic boundary condition for T at $r = 1$, equation (5a), the global heat flux across the outer boundary is obviously zero. Nevertheless, it is possible to introduce an overall Nusselt number of the form

$$Nu = \frac{1}{Nu^*}\int_0^{2\pi}\left|\frac{\partial T}{\partial r}\right|_{r=R}\mathrm{d}\phi \qquad (24)$$

where

$$Nu^* = \int_0^{2\pi}\left|\frac{\partial T_0}{\partial r}\right|_{r=R}\mathrm{d}\phi = 4K_1 \qquad (25)$$

is the overall Nusselt number for pure conduction, with $K_1 = (R^2-1)/(R^3+R)$. Adding together the zero- and first-order terms for the temperature gradient at the outer boundary gives

$$\frac{\partial T}{\partial r} = K_1\cos\phi + \frac{Ra}{R^3} \times [K_2(4\cos^2\phi-3)+K_3]\cos\phi \qquad (26)$$

at $\phi_0 = 0$ and

$$\frac{\partial T}{\partial r} = -K_1 \cos\phi + \frac{Ra}{R^3} \times [K_2(4\cos^2\phi - 3) + K_3]\cos\phi \quad (27)$$

at $\phi_0 = \pi$, where K_2 and K_3 stand for $(1/2)A^2 f'_1(R)$ and $0.25A^2[f'_2(R) + f'_3(R)]$, respectively. Depending on the relative magnitudes of K_1, K_2, K_3 the higher order harmonics may be important enough to reverse the local heat flux more than twice from 0 to 2π. However, it is easy to show that there will be no inversion of the heat flux at $r = R$ over the range $-\pi/2 < \phi < \pi/2$ provided that Ra is small enough. Indeed, a closer examination of equations (26) and (27) reveals that, as long as the condition

$$\frac{Ra}{R^3} \leqslant \frac{|K_1|}{|K_3| + 3|K_2|} \quad (28)$$

is satisfied, equation (26) will be positive and equation (27) negative for any value of ϕ between $-\pi/2$ and $\pi/2$. Assuming that equation (28) holds, it is then a simple matter to evaluate equation (24) from equations (25)–(27) using the symmetry of the problem, which leads to

$$Nu = 1 \pm \frac{Ra}{K_1 R^3}(K_3 - K_2/3). \quad (29)$$

The plus and minus signs in equation (29) correspond to the cases $\phi_0 = 0$ and π, respectively. The upper limit placed upon Ra by equation (28) is equal to 14,488 when $R = 2$ according to the calculation based on equations (17). Thus, the condition imposed by equation (28) is certainly satisfied over the range of validity of the second-order perturbation solution, and therefore equation (29) holds whenever equations (17) hold.

The consequence of a first-order dependence in Ra for the Nusselt number is unusual. As implied by equation (29), the initial effect of convection is to increase or decrease the value of Nu by the same amount depending on whether ϕ_0 is zero or π. The calculations at $Ra = 400$ based on equations (17b) and (29) show that $Nu = 1.003$ for $\phi_0 = \pi$ and 0.997 for $\phi_0 = 0$ at $R = 2$.

Let us consider now the general situation of oblique heating, i.e. $0 < \phi_0 < \pi$. Depending on the values assigned to ϕ_0 and Ra, the flow consists (as mentioned earlier) of either zero, one or two pairs of recirculation cells imbedded in a mainstream around the cavity. At low Ra, ψ_i may be obtained readily from equations (17a) and (18)

$$\psi_i = GA(C_1 + C_4 - 1/64)\sin\phi_0 + \frac{G^2A^2}{2}(\gamma_{4,1} + \gamma_{4,3} + \gamma_{4,5} + \gamma_{4,6} + \gamma_{4,8})\sin(2\phi_0). \quad (30)$$

The first-order contribution shows that the flow rate across the annulus varies sinusoidally with the heating angle, reaching therefore a maximum value when heating is from the side at $\phi_0 = \pi/2$. The second-order contribution shows that a maximum flow rate is obtained when the heating angle is greater than $\pi/2$.

Figures 2–5 provide a comparison between the perturbation and the numerical solutions. Figure 2 shows the variation of the flow rate with the heating angle

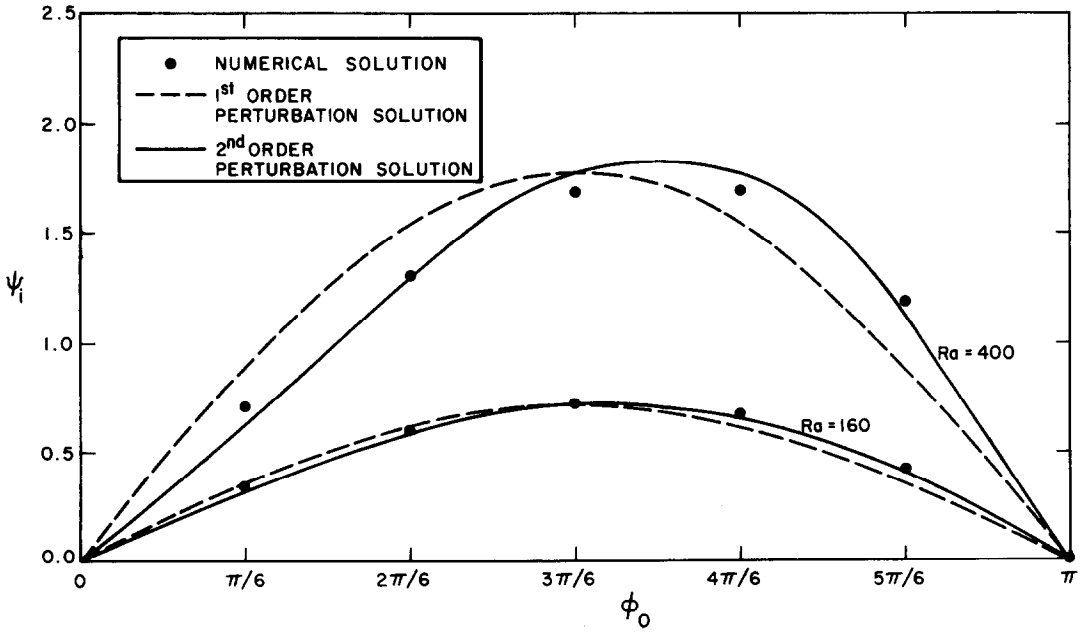

FIG. 2. Circulating flow around the cavity. Comparison between analytical and numerical results, $R = 2$, $Pr = 1$.

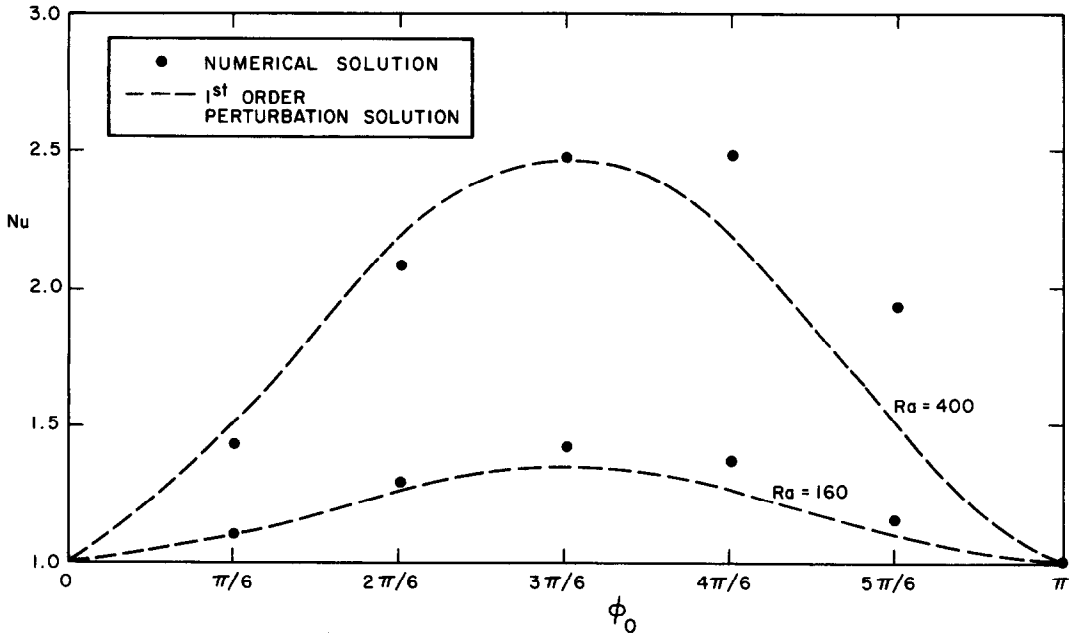

FIG. 3. Nusselt number. Comparison between analytical and numerical results, $R = 2$, $Pr = 1$.

at $Ra = 160$ and 400 for $R = 2$ and $Pr = 1$ together with the corresponding results calculated from the numerical solution procedure described in the previous section. The asymmetry introduced by the second-order term in equation (29) is obvious. Figure 3 presents the overall Nusselt number profiles for the same values of Ra, R and Pr. The analytical results based on the first-order solution for T are symmetric with respect to $\phi_0 = \pi/2$, while the numerical results are not.

Figures 4 and 5 show the variation of ψ_i and Nu respectively with Ra and R, for $\phi_0 = \pi/2$. From these two figures, and also to a certain extent from the previous two (for $R = 2$), it can be asserted that the low order perturbation solution for ψ and T given here is accurate up to $Ra = 400$ or 500 for $R = 2$, up

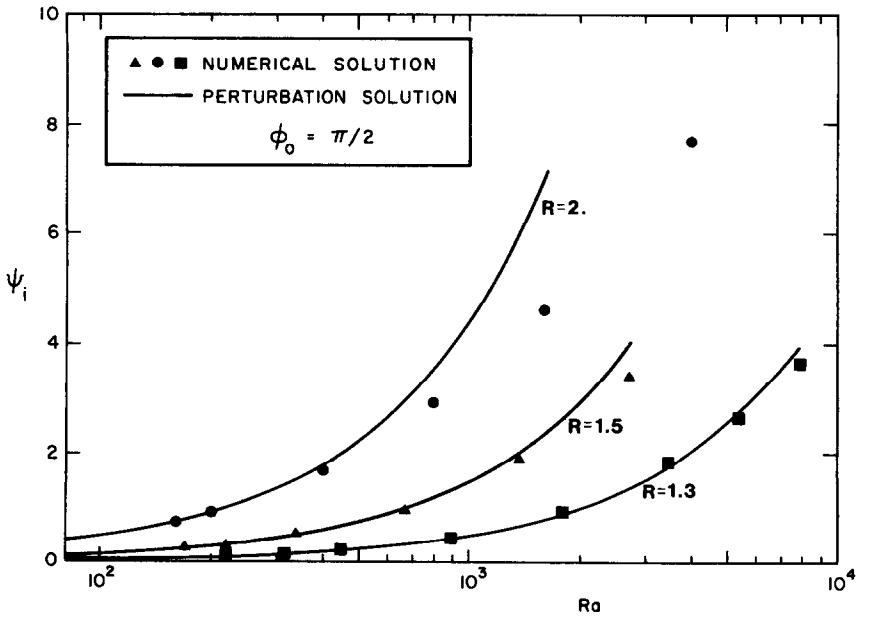

FIG. 4. Circulating flow at $\phi_0 = \pi/2$ as a function of Ra. Analytical and numerical results, $R = 1.3$, 1.5, 2, $Pr = 1$.

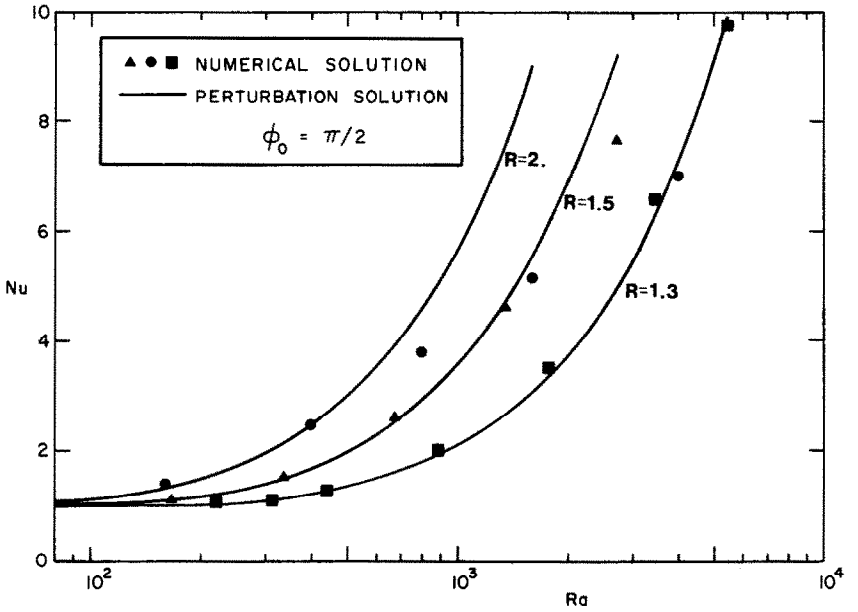

FIG. 5. Nusselt number at $\phi_0 = \pi/2$ as a function of Ra. Analytical and numerical results, $R = 1.3, 1.5, 2$.

to $Ra = 1300$ or 1400 for $R = 1.5$ and up to $Ra = 5000$ or 5500 for $R = 1.3$.

The computations presented in Figs. 4 and 5 were repeated for $Pr = 0.7$ and 7. As expected, the influence of this parameter was almost negligible over the range of Rayleigh numbers considered. For instance, for $R = 2$ and $Ra = 1600$, the numerically computed value of $Pr\,\psi_i$ changed from 4.592 ($Pr = 0.7$) to 4.664 ($Pr = 7$) which is of the order of 1.5%. It is obvious from equation (30) that $Pr\,\psi_i$ is a function of Ra only, up to the second order for $\phi_0 = \pi/2$, and that the perturbation solution remained unaffected.

4.2. *Convective regime*

As the Rayleigh number is increased, the perturbation solutions become inappropriate and the problem must be investigated numerically. The numerical solutions reveal the existence of various flow regimes depending on the value of the Rayleigh number and the heating angle ϕ_0. All the results which are presented in this subsection were obtained for an aspect ratio $R = 2$, assuming a Prandtl number value $Pr = 1$.

4.2.1. *Heating from the top.* This case corresponds to a stable stratification. A steady-state symmetric non-recirculating flow is observed over the entire range of Rayleigh numbers considered in this study ($0 < Ra < 40{,}000$). The streamlines invariably form a quadri-cellular pattern. As the Rayleigh number is increased however, the isotherms become more and more horizontal compared to the pseudo-conduction situation. The overall heat transfer behavior described by equation (24) remains comparable to that which is found in the absence of strong convection effects.

4.2.2. *Heating from the bottom.* This situation corresponds to an unstable stratification. Three distinct subregimes can be obtained in this case depending on the value of Ra.

For $Ra < 1120$, the flow is again quadricellular without recirculation and does not differ significantly from the stably stratified flow. Above this threshold value, a net circulation suddenly develops around the annulus and the symmetry with respect to the X- and Y-axes is lost. The flow and temperature fields do remain centro-symmetric however. In fact, this circulation is a consequence of the potentially unstable behavior of a fluid layer heated from below just like in the classical Bénard problem.

Associated with the development of the instabilities is an abrupt change in the flow rate and heat transfer. The streamlines are concentric circles in the beginning of the circulating flow regime and become progressively oval as Ra increases. When Ra increases beyond roughly 11,000, secondary cells begin to appear, near the outer boundary at first, then also near the inner boundary. Figure 6 shows the evolution of ψ_i with Ra. Figure 7 describes how the heat transfer with the surroundings is enhanced by the net circulation (i.e. ψ_i) around the cavity. The 'leveling-off' effect which is observed on both Figs. 6 and 7 at high Rayleigh numbers might be due to a progressive balance between the mainstream and reverse flows. Indeed, the flows are initially quite weak in the secondary cells, but eventually they increase, and become comparable to the mainstream flow. Finally, beyond a second critical Rayleigh number, whose value is slightly above 40,000, no steady-state solution can be reached. The time-dependence is very weak at first

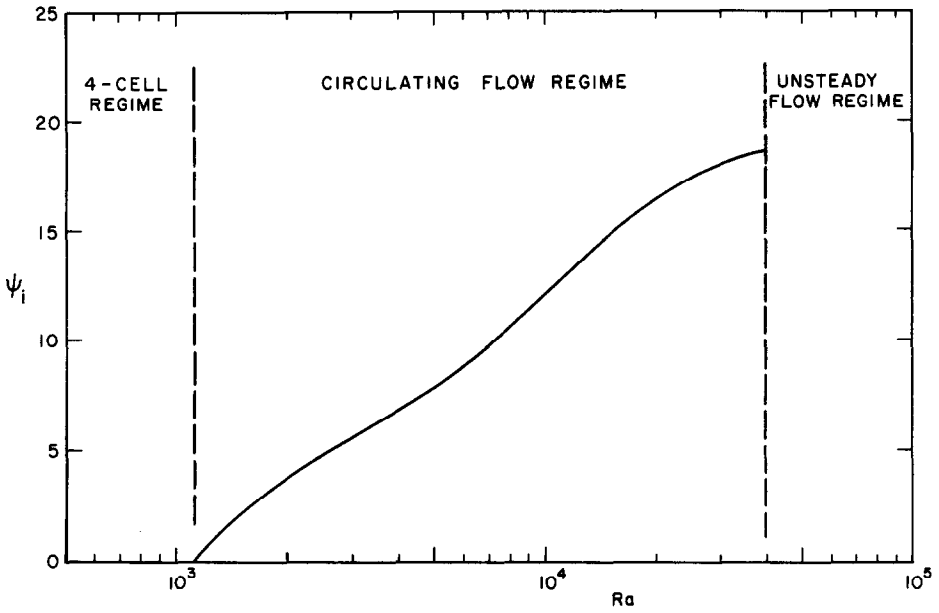

FIG. 6. Circulating flow at $\phi_0 = \pi$ as a function of Ra, $R = 2$, $Pr = 1$.

and it is not clear whether or not this time dependence is periodic in character. As the Rayleigh number increases, the oscillations become faster and their amplitude grows. A detailed investigation of the unsteady flow regime was beyond the reach of the authors' computer code capability and was consequently omitted.

4.2.3. *Arbitrary heating angle.* In this case there is always a net circulation around the annular cavity, except of course for $\phi_0 = 0$ (and π, at low Ra). The maximum flow and heat transfer rates are obtained for a heating angle below the horizontal whose value depends on Ra. The tendencies towards asymmetry which were revealed by the perturbation analysis are corroborated by the numerical solutions. Leaving aside the case $\phi_0 = \pi$, flow reversals can occur in an ever wider range of heating angles as Ra is increased. In fact, for $Ra = 15{,}000$, weak secondary cells are

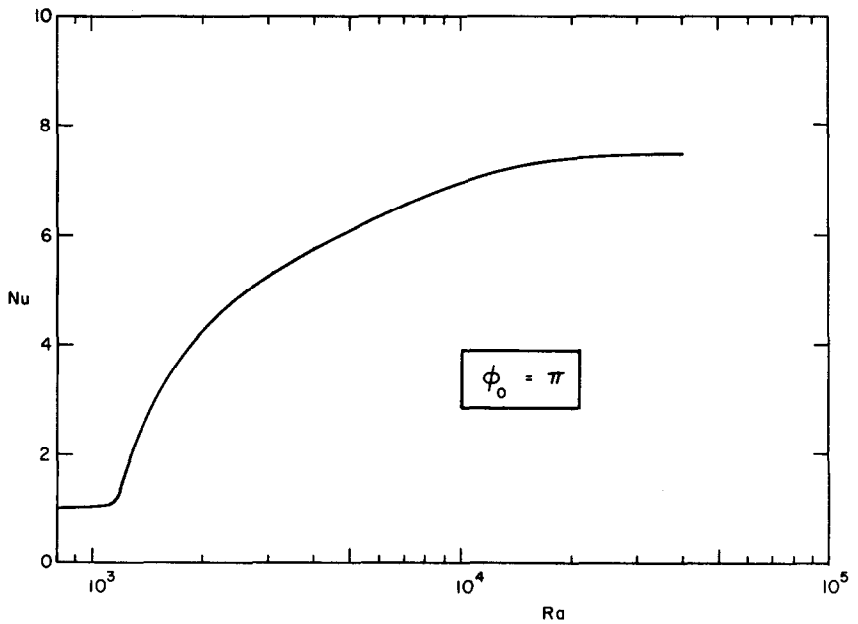

FIG. 7. Nusselt number at $\phi_0 = \pi$ as a function of Ra, $R = 2$.

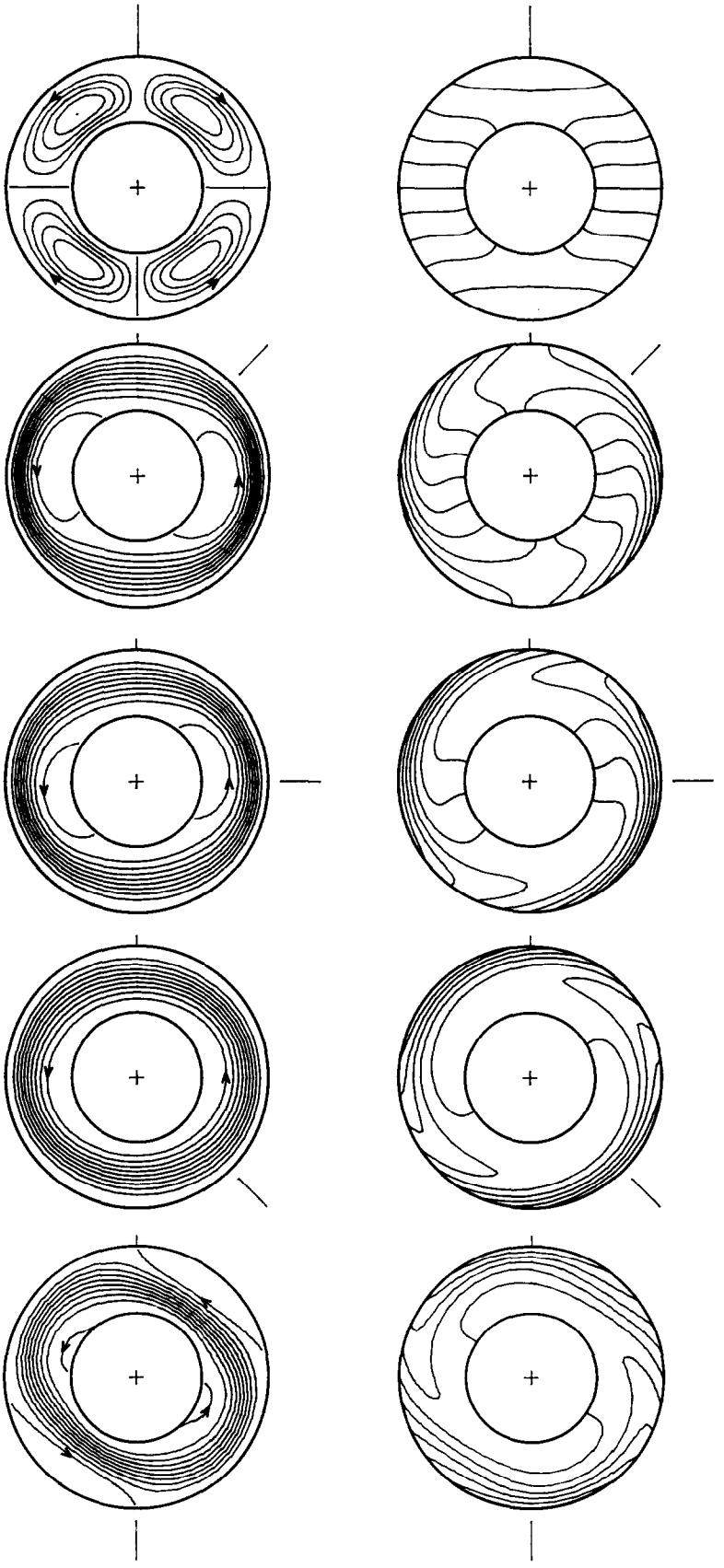

FIG. 8. Flow and temperature fields as function of ϕ_0, $Ra = 40{,}000$, $R = 2$, $Pr = 1$.

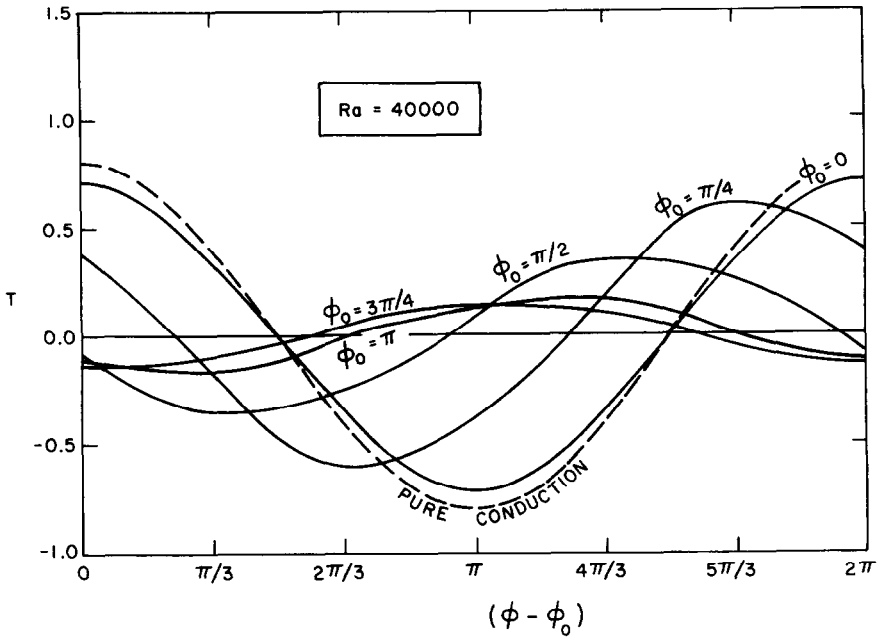

FIG. 9. Temperature distribution on the inner wall as a function of ϕ_o, $Ra = 40{,}000$, $R = 2$, $Pr = 1$.

present at the inner boundary even when heating is from the side at $\phi_o = \pi/2$. Figure 8 depicts the flow and temperature fields for $Ra = 40{,}000$ at different heating angles and clearly shows the secondary cells. The corresponding temperature distributions at the inner wall may be seen on Fig. 9. The pure conduction temperature distribution, given by the dashed line, stands for all ϕ_o. The temperature profiles reveal a degree of asymmetry with respect to $\phi - \phi_o = \pi/2$ which is directly related to the magnitude of ψ_i, reaching a maximum when ϕ_o is between $3\pi/4$ and π.

Figure 10 shows the variation of the flow rate ψ_i

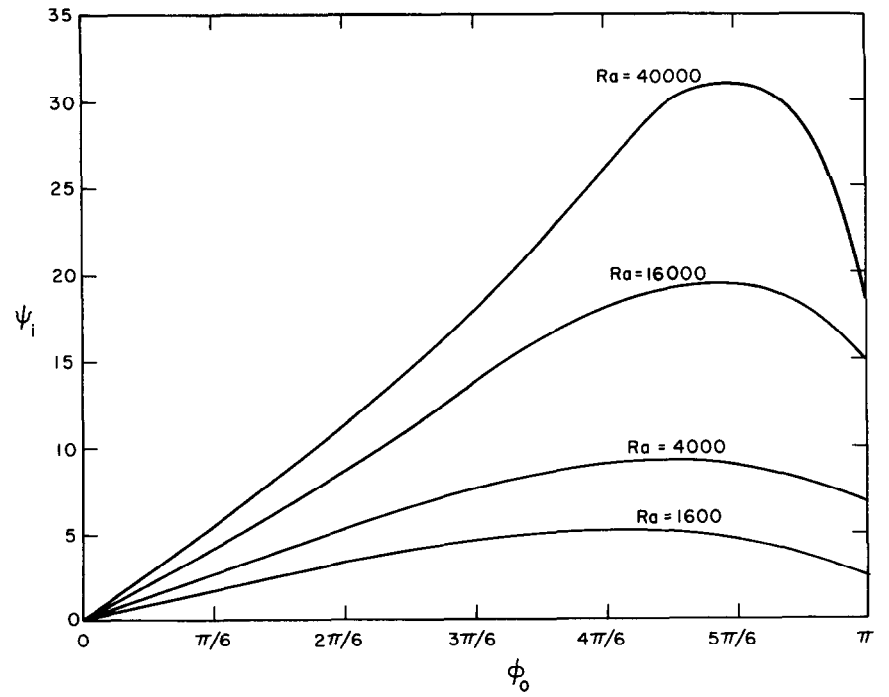

FIG. 10. Circulating flow as a function of ϕ_o, $R = 2$, $Pr = 1$.

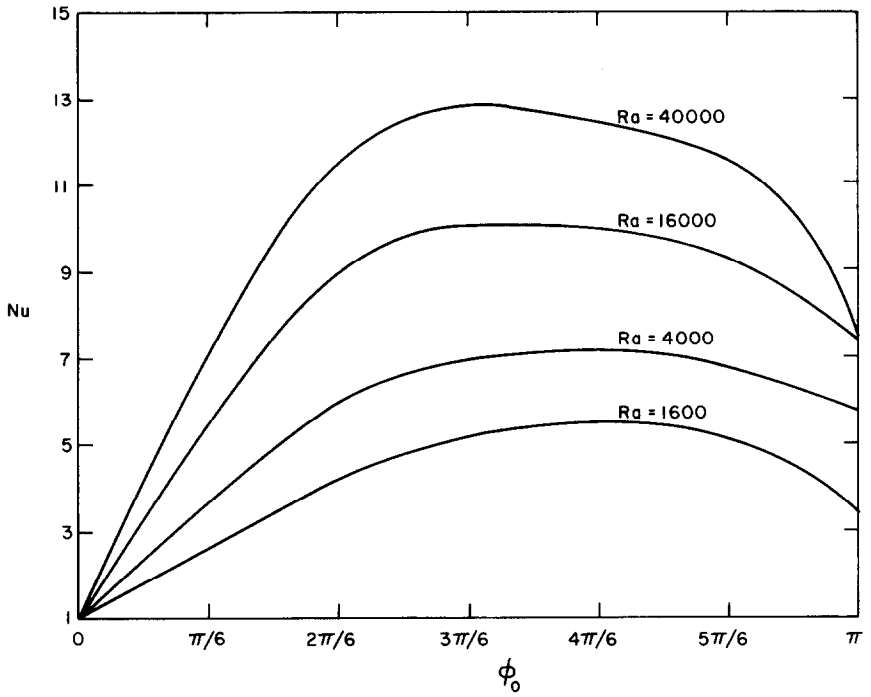

FIG. 11. Nusselt number as a function of ϕ_0, $R = 2$.

with the heating angle ϕ_0 for different values of *Ra*. The asymmetry of the ψ_i profiles with respect to $\phi_0 = \pi/2$ becomes more and more pronounced as *Ra* increases. Figure 11 shows the corresponding Nusselt number profiles, *Nu* vs ϕ_0. It is quite interesting to notice the shift in the location of the maximum *Nu* away from $\phi_0 = \pi/2$ at small Rayleigh numbers (see Fig. 3) and then backwards towards $\phi_0 = \pi/2$ at large Rayleigh numbers. This effect is probably also explained by the balance mechanism between the main flow and the recirculating flow near the outer boundary which hinders heat transfer at large values of ϕ_0 and *Ra*. In particular, the 'leveling-off' effect mentioned earlier for *Nu* at $\phi_0 = \pi$ becomes obvious on Fig. 11.

5. CONCLUDING REMARKS

Natural convection flow in an annular fluid layer has been investigated assuming adiabatic conditions at the inner boundary and a prescribed sinusoidal temperature at the outer boundary. Two-dimensional steady-state solutions were obtained with regular perturbation and numerical methods.

The perturbation solutions show that the first effect of incipient convection is to decrease the value of the overall Nusselt number for $\phi_0 = 0$, which is verified numerically. This phenomenon has been described previously by Robillard *et al.* [10] for $\phi_0 = \pi$ in porous flow with an isothermal inner boundary. As opposed to the case of the porous medium [9], there exists for the fluid medium a wider range of heating angles for which no separation will occur in the limit of small Rayleigh numbers.

Just as in the porous case [9], the present study concludes to the existence of various flow regimes depending on the values of the Rayleigh number and the heating angle. However, unlike the porous case, the heat flow at the outer boundary never changed sign more than twice on $0 \leqslant \phi < 2\pi$ over the whole range of Rayleigh numbers considered ($0 < Ra < 40{,}000$). Furthermore, it was reported in ref. [9] that for the porous medium the heat flow across the outer boundary is more and more concentrated at the top and bottom of the cavity as *Ra* is increased. This tendency is still present for the fluid medium, but it is far less pronounced. Finally, it is mentioned in ref. [9] that the flow rate ψ_i reached a maximum and then decreased with *Ra* for $\phi_0 = \pi$. This is in contrast with the monotonous increase of ψ_i with *Ra* which is observed for a fluid.

It might be stated as final remark that the physical behavior of the fluid medium is not as easily understood as that of the porous medium. In the latter case, there is a simple relation between the net circulation around any closed path in the flow and the temperature field which has no counterpart in the case of a fluid. For instance in ref. [9] the existence of recirculating cells such as the ones shown on Fig. 8, $\phi_0 = \pi$, may be deduced *a priori* from the fact that the

circulation on the outer boundary takes the value zero.

Acknowledgement—This research was supported by the National Research Council of Canada through grants NRC A 4197 and NRC A 9201.

REFERENCES

1. D. Japikse, Advances in thermosyphon technology. In *Advances in Heat Transfer*, Vol. 9, pp. 1–111. Academic Press, New York (1973).
2. P. Welander, On the oscillatory instability of a differentially heated fluid loop, *J. Fluid Mech.* **29,** 17–30 (1967).
3. H. F. Creveling, J. F. de Paz, J. Y. Baladi and R. J. Schoenhals, Stability characteristics of a single-phase free convection loop, *J. Fluid Mech.* **67,** 65–84 (1975).
4. P. S. Damerell and R. J. Schoenhals, Flow in a toroidal thermosyphon with angular displacement of heated and cooled sections, *J. Heat Transfer* **101,** 672–675 (1979).
5. A. Mertol, R. Greif and Y. Zvirin, Two dimensional study of heat transfer and fluid flow in a natural convection loop, *ASME J. Heat Transfer* **104,** 508–514 (1982).
6. A. Mertol, R. Greif and T. Zvirin, Two dimensional analysis of transient flow and heat transfer in a natural circulation loop, *Wärme- u. Stoffeübertr.* **18,** 89–98 (1984).
7. S. N. Singh and J. M. Elliot, Free convection between horizontal concentric cylinders in a slightly thermally stratified fluid, *Int. J. Heat Mass Transfer* **22,** 639–646 (1979).
8. L. Robillard, T. H. Nguyen and P. Vasseur, Free convection in a two dimensional porous loop, *ASME J. Heat Transfer* **108,** 277–283 (1986).
9. L. Robillard, T. H. Nguyen, M. G. Satish and P. Vasseur, Free convection in a non-uniformly heated annular porous layer, ASME Winter Annual Meeting, ASME Paper 85-WA/H7-8 (1985).
10. L. Robillard, T. H. Nguyen, M. G. Satish and P. Vasseur, Oscillating flow in an annular porous layer heated from below, ASME 23rd Nat. Heat Trans. Conf. Denver, Colorado, U.S.A., H7D46, pp. 41–47 (1985).
11. P. Vasseur, L. Robillard and B. C. Shekar, Natural convection of water within a horizontal cylindrical annulus with density inversion, *ASME J. Heat Transfer* **105,** 117–123 (1983).

APPENDIX

The coefficients for the first-order stream function ψ, equation (17a), are

$$C_1 = \frac{6-5R^2-R^4+4\ln R(-3+R^2+4\ln R)}{64(1-R^{-2})}$$

$$C_2 = \frac{1-4\ln R-R^2}{16(1-R^{-2})}$$

$$C_3 = -1/8$$

$$C_4 = 1/32-C_2/2-C_3/2$$

$$C_5 = \frac{R^{-2}+R^{-4}}{32(1-R^{-2})^2} + \frac{-R^{-4}+R^{-6}}{8(1-R^{-2})^4}\ln R$$

$$C_6 = \frac{-1-4R^{-2}-R^{-4}}{32(1-R^{-2})^2} + \frac{1+3R^{-4}-4R^{-6}}{16(1-R^{-2})^4}\ln R$$

$$C_7 = \frac{3(1+R^{-2})}{32(1-R^{-2})^2} + \frac{-1+R^{-6}}{8(1-R^{-2})^4}\ln R$$

$$C_8 = -C_5-C_6-C_7.$$

The functions $f_i(r)$ in the first-order temperature function T_1, equation (17b), are given by the following expressions:

$$f_1(r) = \alpha_{11}r^3+\alpha_{12}r^{-3}+\alpha_{13}r^5+\alpha_{14}r^3\ln r + \alpha_{15}r+\alpha_{16}r^{-1}+\alpha_{17}r\ln r$$

$$f_2(r) = \alpha_{21}r+\alpha_{22}r^{-1}+\alpha_{23}r^{-1}\ln r+\alpha_{24}r\ln r + \alpha_{25}r^3\ln r+\alpha_{26}r\ln^2 r+\alpha_{27}r^3+\alpha_{28}r^5$$

$$f_3(r) = \alpha_{31}r+\alpha_{32}r^{-1}+\alpha_{33}r^5+\alpha_{34}r^3+\alpha_{35}r\ln r + \alpha_{36}r^{-1}\ln r+\alpha_{37}r^{-3}+\alpha_{38}r\ln^2 r.$$

For the second-order stream function ψ_2, equation (18), the functions $g_i(r)$ are given by

$$g_1(r) = \gamma_{1,1}r^6+\gamma_{1,2}r^4+\gamma_{1,3}r^{-2}+\gamma_{1,4}r^{-4}+\gamma_{1,5}r^6\ln r + \gamma_{1,6}r^8+\gamma_{1,7}+\gamma_{1,8}r^4\ln r+\gamma_{1,9}r^4\ln^2 r+\gamma_{1,10}r^2 + \gamma_{1,11}r^2\ln r$$

$$g_2(r) = \gamma_{2,1}r^4+\gamma_{2,2}r^2+\gamma_{2,3}+\gamma_{2,4}r^{-2}+\gamma_{2,5}r^6+\gamma_{2,6}r^8 + \gamma_{2,7}\ln r+\gamma_{2,8}r^6\ln r+\gamma_{2,9}r^4\ln r+\gamma_{2,10}r^4\ln^2 r + \gamma_{2,11}r^2\ln r+\gamma_{2,12}r^2\ln^2 r$$

$$g_3(r) = \gamma_{3,1}r^4+\gamma_{3,2}r^2+\gamma_{3,3}+\gamma_{3,4}r^{-2}+\gamma_{3,5}r^6+\gamma_{3,6}r^8 + \gamma_{3,7}\ln r+\gamma_{3,8}r^6\ln r+\gamma_{3,9}r^4\ln r+\gamma_{3,10}r^4\ln^2 r + \gamma_{3,11}r^2\ln r+\gamma_{3,12}r^2\ln^2 r$$

$$g_4(r) = \gamma_{4,1}+\gamma_{4,2}\ln r+\gamma_{4,3}r^2+\gamma_{4,4}r^2\ln r+\gamma_{4,5}r^6 + \gamma_{4,6}r^8+\gamma_{4,7}r^6\ln r+\gamma_{4,8}r^4+\gamma_{4,9}r^4\ln r + \gamma_{4,10}r^2\ln^2 r+\gamma_{4,11}r^4\ln^2 r.$$

For the sake of brevity, the coefficients α_{ij} and $\gamma_{i,j}$ are not given explicitly here, but are available from the authors upon request.

ETUDE DE LA CONVECTION LAMINAIRE NATURELLE DANS UNE COUCHE FLUIDE ANNULAIRE NON UNIFORMEMENT CHAUFFEE

Résumé—On étudie la convection naturelle relative à une couche annulaire confinée entre deux cylindres horizontaux. Des résultats sont présentés pour le cas d'une frontière intérieure adiabatique avec une distribution de température sinusoïdale sur la frontière extérieure. Le problème est formulé avec l'approximation de Boussinesq et il est résolu en utilisant les techniques de perturbation et de différences finies. On trouve que ces deux méthodes sont en bon accord pour la convection faible. On constate l'existence de plusieurs régimes d'écoulement qui dépendent de *Ra* et de la position angulaire du maximum de température sur la frontière extérieure, ce qui est semblable à des résultats antérieurs pour le milieu poreux. En particulier quand on chauffe par le bas, il y a trois sous-régimes distincts dans le domaine de paramétres considéré ($R = 2$, $0 < Ra < 40\,000$): l'écoulement stable à quatre cellules pour $Ra < 1120$, l'écoulement recirculant avec ou sans cellules secondaires pour $1120 < Ra < 40\,000$, et finalement un écoulement recirculant instable pour $Ra > 40\,000$. Des cellules secondaires commencent à apparaître près de la limite extérieure à $Ra = 11\,000$. Pour un angle quelconque de chauffage, il y a toujours une recirculation nette autour de la cavité, à moins que le chauffage soit au sommet, qui conduit à une augmentation du transfert de chaleur avec l'environnent. Ce maximum de mouvement et de transfert est obtenu pour un angle de chauffage au-dessous de l'horizontale mais qui dépend de *Ra*.

UNTERSUCHUNG DER LAMINAREN NATÜRLICHEN KONVEKTION IN EINEM UNGLEICHMÄSSIG BEHEIZTEN RINGRAUM

Zusammenfassung—Die freie Konvektion in einem fluidgefüllten Ringraum zwischen zwei konzentrischen Zylindern wird untersucht. Ergebnisse werden für den Fall des adiabaten inneren Zylinders und einer sinusförmigen Temperaturverteilung auf dem äußeren Zylinder gezeigt. Das Problem wird mit Hilfe der Boussinesq-Näherung formuliert und mit Hilfe von Differenzenverfahren und Strömungsverfahren gelöst. Beide Verfahren zeigen vor allem bei schwach ausgeprägter Konvektion gute Übereinstimmung. Die Lösungen zeigen verschiedene Strömungsarten auf, abhängig von der Rayleigh-Zahl und dem Ort der höchsten Temperatur auf dem äußeren Zylinder. Sie sind früheren Ergebnissen mit poröser Füllung prinzipiell ähnlich. In einem Fall zeigt sich, daß die gerade einsetzende Konvektion die Nusselt-Zahl verringert. Wenn direkt von unten beheizt wird, erhält man im Bereich der untersuchten Parameter (Radienverhältnis $R_1/R_2 = 2$, Rayleigh-Zahl $0 < Ra < 40\,000$) drei verschiedene Strömungsarten: stationäre Rechteckzellen für $Ra < 1120$, Zirkulationsströmung mit und ohne Sekundärzellen für $1120 < Ra < 40\,000$ und schließlich instationäre Zirkulationsströmung für $Ra > 40\,000$. Sekundärzellen entstehen nahe der äußeren Zylinderwand ab etwa $Ra = 11\,000$. Bei allen anderen Winkelpositionen der höchsten Temperatur erhält man eine umlaufende Strömung im Ringraum, außer wenn direkt von oben geheizt wird. Dies führt zu einem verstärkten Wärmeübergang an die Umgebung. Die stärkste Strömung und den besten Wärmeübergang erhält man, wenn die Stelle maximaler Temperatur auf der unteren Zylinderhälfte ist, wobei die genaue Position von der Rayleigh-Zahl abhängt.

ИССЛЕДОВАНИЕ ЛАМИНАРНОЕ ЕСТЕСТВЕННОЙ КОНВЕКЦИИ В КОЛЬЦЕВОМ СЛОЕ ЖИДКОСТИ ПРИ НЕРАВНОМЕРНОМ НАГРЕВЕ

Аннотация—Изучалась свободная конвекция в кольцевом слое жидкости, находящейся между двумя горизонтальными цилиндрами. Представлены результаты для адиабатической внутренней границы и синусоидального распределения температуры на внешней границе слоя. Использовалось приближение Буссинеска. Решение получено методом возмущений и численным методом конечных разностей. Обнаружено, что результаты, полученные обоими методами, хорошо согласуются для случая слабой конвекции. Решения показывают существование различных режимов течения, зависящих от числа Ra и углового положения максимума температуры на наружной границе, которые сходны по характеру с полученными ранее результатами для пористой среды. Найдено, что в начальный период возникающая конвекция может приводить к уменьшению числа Нуссельта. В частности, при нагреве снизу могут быть получены три отчетливых подрежима в области рассматриваемых параметров ($R = 2$, $0 < Ra < 40\,000$), а именно: стационарное течение с четырьмя ячейками для $Ra < 1120$, циркуляционное течение со вторичными ячейками и без них для $1120 < Ra < 40\,000$, и наконец, неустойчивое циркуляционное течение для $Ra > 40\,000$. Вторичные ячейки появляются вблизи наружной границы при $Ra = 11\,000$. При произвольном положении максимума температуры всегда существует чисто циркуляционное течение в полости до тех пор, пока не начинает греться верх, что приводит к усилению теплообмена. Максимумы скорости течения и коэффициента теплообмена зависят от числа Ra и наблюдались при положении максимума температуры ниже оси.